Nectin-4 reduces T cell effector function and is a therapeutic target in pancreatic cancer

Max Heiduk[1,2*], Carolin Beer[1*], Sarah Cronjaeger[1,2], Emily A. Kawaler[3], Ulrich Sommer[4,5], Franziska Baenke[1,2,6], David Digomann[1,2,6], Loreen Natusch Bufe[1,2,6], Charlotte Reiche[1,2], Jessica Glück[1], Franziska Hoffmann[1], Sungsik Kim[7], Daniel E. Stange[1,2,6], Diane M. Simeone[7], Jürgen Weitz[1,2,6], Lena Seifert[1,2,6#], and Adrian M. Seifert[1,2,6#]

[1] Department of Visceral, Thoracic and Vascular Surgery, University Hospital Carl Gustav Carus, Technische Universität Dresden, Dresden, Germany.
[2] National Center for Tumor Diseases (NCT), Dresden, Germany: German Cancer Research Center (DKFZ), Heidelberg, Germany; Faculty of Medicine and University Hospital Carl Gustav Carus, Technische Universität Dresden, Dresden, Germany; Helmholtz-Zentrum Dresden - Rossendorf (HZDR), Dresden, Germany
[3] Perlmutter Cancer Center, NYU Langone Health, New York, New York, USA
[4] Institute of Pathology, Faculty of Medicine Carl Gustav Carus, Technische Universität Dresden, Dresden, Germany.
[5] National Center for Tumor Diseases (NCT), Biobank Dresden, University Hospital Carl Gustav Carus, Technische Universität Dresden, Dresden, Germany.
[6] German Cancer Consortium (DKTK), Partner Site Dresden, German Cancer Research Center (DKFZ), Heidelberg, Germany.
[7] Department of Surgery, UC San Diego Health, San Diego, CA, USA; Moores Cancer Center, UC San Diego Health, San Diego, CA, USA.
[*] Co-first authors
[#] Co-senior authors

Correspondence: Adrian Seifert, Department of Visceral, Thoracic and Vascular Surgery, University Hospital Carl Gustav Carus, Technische Universität Dresden, Fetscherstr. 74, 01307 Dresden, Germany, Email: adrian.seifert@ukdd.de, Tel: +49 351 4580

Disclosure: All authors declare no potential conflicts of interest.

Running title: Nectin-4 in pancreatic cancer
Word Count: 2635
Figures: 6
Supplementary Material: 3 Supplementary Figures, 6 Supplementary Tables
Key words: Pancreatic cancer, TIGIT, Nectin-4, tumor-infiltrating T cells

ABSTRACT

Pancreatic ductal adenocarcinoma (PDAC) has a dismal prognosis and current therapies show limited efficacy. Ligands and receptors of the TIGIT axis were analyzed using multicolor flow cytometry of tumor and blood samples, immunohistochemistry from primary tumors, and single-cell RNA sequencing from primary tumors and liver metastasis from patients with various stages of PDAC. The effect of soluble and plate-bound Nectin-4 on T cell function was tested *in vitro*. Further, patient-derived PDAC organoids were treated with the standard of care therapies FOLFIRINOX, gemcitabine plus paclitaxel, or the antibody-drug conjugate enfortumab vedotin. TIGIT expression was increased on tumor-infiltrating conventional and regulatory T cells compared with T cells from matched blood. Nectin-4, but not CD155 expression was associated with poor outcome. Nectin-4 was exclusively expressed by tumor cells and correlated with low immune infiltration. Notably, Nectin-4 inhibited T cell effector cytokine production *in vitro*. Targeting Nectin-4 with the antibody-drug conjugate enfortumab vedotin inhibited tumor growth in multiple patient-derived PDAC organoids. Collectively, our data underscores Nectin-4 as a novel therapeutic target and provides the rationale to test this agent in PDAC patients.

BRIEF SUMMARY

Nectin-4 is associated with poor outcome and low immune infiltration, and reduces T cell effector function. Nectin-4 is a novel therapeutic target and can be effectively targeted with enfortumab vedotin.

INTRODUCTION

Pancreatic ductal adenocarcinoma (PDAC) is one of the deadliest malignancies, with a 5-year survival rate across all tumor stages of only 13% (1). Immunotherapies targeting immune checkpoint receptors (ICRs) have revolutionized cancer treatment, but have not yet shown efficacy in PDAC due to a highly immunosuppressive tumor immune microenvironment and poor immunogenicity (2). Intratumoral T cells in PDAC are mostly dysfunctional and exhausted (3). Nevertheless, increased infiltration of effector T cells and a pro-inflammatory, anti-tumorigenic immune infiltrate are associated with improved survival in PDAC, suggesting potential for immunotherapies (4). The TIGIT axis comprises a network of lymphocyte-expressed ICRs, such as TIGIT, CD226 and CD96, which interact with the ligands CD155 and members of the Nectin family (5). Recently, we identified TIGIT as a marker of exhausted $CD8^+$, conventional $CD4^+$ (Tconvs) and immunosuppressive regulatory T cells (Tregs) in PDAC (6-8). In a neoantigen-expressing PDAC mouse model, CD155 overexpression led to immune evasion, which was overcome with combinational immunotherapy of anti-PD-1, anti-TIGIT and agonistic CD40 antibody treatment (9). While previous studies have mainly focused on TIGIT and CD155 as one of its ligands, a comprehensive understanding of the axis is still needed to evaluate its potential for future immunotherapeutic strategies in PDAC. Our data reshape the understanding of the TIGIT axis in PDAC by underscoring Nectin-4 expression as a major mechanism of immune escape and therapeutic target in PDAC.

RESULTS

TIGIT, CD226, and CD96 are expressed by tumor-infiltrating T cells.

To identify the distribution of receptors and ligands of the TIGIT axis in the pancreatic tumor microenvironment, we analyzed the known receptors of the the TIGIT axis. TIGIT, CD226, and CD96 are important immune regulatory receptors involved in modulating T cell activity in anti-tumor immunity (10). The expression of these receptors by T cells isolated from blood and matched PDAC tumor samples was analyzed by multicolor flow cytometry (**Fig. 1A-C**). Patient characteristics are shown in **Supplementary Table S1**. TIGIT was highly expressed by Treg in blood and PDAC and significantly increased in Tconv and Treg in PDAC compared to blood (**Fig. 1A**). CD226 expression by intratumoral $CD8^+$ T cells and Treg (**Fig. 1B**), and CD96 expression by Tconv was significantly reduced in PDAC (**Fig. 1C**). While the distribution of the ICR co-expressing subsets of $CD8^+$ T cells was largely similar between blood and PDAC, $TIGIT^-CD226^+CD96^+$ cells constituted the main subset among blood Tconv, but was significantly decreased in PDAC (**Fig. 1D**). All TIGIT-expressing subsets were significantly increased among PDAC Tconv. $TIGIT^+CD226^-CD96^+$ Treg were increased in PDAC, whereas Treg with no expression of these ICRs were almost absent in PDAC. Notably, TIGIT and CD96 expression showed a strong positive correlation between T cell subsets in blood and PDAC (**Fig. 1E**; **Supplementary Table S2, S3**). CD226 and TIGIT expression by $CD8^+$ T cells in PDAC correlated negatively. Furthermore, different transcription factors were investigated to assess their association with ICR expression (**Supplementary Fig. S1D-F**). Representative gating is shown in **Supplementary Fig. S1A-C**. The proliferation marker Ki-67 was particularly high among $CD226^+$ Treg, but also significantly increased among $TIGIT^+$ $CD8^+$ T cells and $TIGIT^+$ Tconv, indicating an increased proliferation of these subsets (**Supplementary Fig. S1D**). Eomesodermin (Eomes), which drives $CD8^+$ T cell exhaustion (11), was significantly higher in $TIGIT^+$, but lower in $CD226^+$ and $CD96^+$ $CD8^+$ T cells (**Supplementary Fig. S1E**). Most interestingly, GATA3, a transcription factor known to drive the differentiation towards a rather anti-inflammatory and tumor-protective phenotype (12), was significantly increased among $TIGIT^+$ $CD8^+$ T cells and Tconv, but not associated with expression of the other ICRs

(**Supplementary Fig. S1F**). In the blood, T cells present significantly different phenotypes based on their ICR expression with Ki-67, Eomes, and GATA3 expression being associated with TIGIT positivity.

Nectin-4 expression is associated with poor outcome in PDAC.

Subsequently, the expression and prognostic relevance of the TIGIT ligands, namely *PVR* (CD155), *PVRL1* (Nectin-1), *PVRL2* (Nectin-2), *PVRL3* (Nectin-3) and *PVRL4* (Nectin-4) was examined using the TCGA dataset (**Supplementary Fig. S2A, B**). Intriguingly, high *PVR* expression was associated with significantly improved overall survival in PDAC, whereas *PVR* and *PVRL1* expression was linked to reduced survival in hepatocellular carcinoma. Most interestingly, while *PVRL4* expression was associated with favorable survival in gastric cancer, it was associated with reduced survival in PDAC. These differences suggest disease-specific prognostic relevance of these proteins. Based on this data, our analyses focused on CD155 and Nectin-4. The correlation between *PVRL4* expression and that of several genes of interest was investigated within the TCGA data set (**Supplementary Fig. S2C**). *PVRL4* showed a positive correlation with *PVRL2*, but was negatively associated with immune cell-related genes, particularly T and NK cell genes, and to a lesser extent with different myeloid cell genes. The expression of *PVRL4* and ICR genes, which are predominantly expressed by T cells, consistently showed a negative correlation. The lowest correlation coefficient between *PVRL4* and any immune-associated gene was with *CD226* (r = -0.560). In contrast, *PVRL4* correlated positively with *LGALS3* (Galectin-3), another ligand known to be involved in immune escape in PDAC (13), and two epithelial genes representative of ductal tumor cells. There was no or a negative association with genes related to fibroblasts or extracellular matrix formation, indicating that Nectin-4 is mainly expressed by tumor cells rather than within the stromal compartment. *PVRL2* also positively correlated with *PVR* and was the only ligand that showed a minor negative correlation with immune-related genes (**Supplementary Table S4**). By immunohistochemistry, tumor cells showed a distinct CD155 and Nectin-4 staining pattern (**Fig. 2A**). No significant differences in expression between the tumor core and periphery were

detected, nor was any association observed with other histological features. The intensity and percentage of positive tumor cells were scored to calculate the immune reactive scores (IRS, **Fig. 2B**). An IRS of 0-4 was classified to be low and an IRS of 6-12 as high expression. Of note, Nectin-4 staining was absent in only 2 of the 68 patients (2.9 %). Approximately 70 % of PDAC samples had high and very high Nectin-4 expression, whereas CD155 had a low intensitiy in more than 60 % of the samples (**Fig. 2C**). CD155 was not significantly associated with prognosis in the univariate analysis, but high Nectin-4 expression was strongly associated with reduced survival of PDAC patients (**Fig. 2D**). Notably, in the multivariate analysis, high CD155 expression was significantly associated with increased survival, while high Nectin-4 expression was a significant risk for reduced survival (**Fig. 2E**). No significant association was observed between expression of either gene and any clinicopathologic characteristics, but metastatic PDAC patients did tend toward increased Nectin-4 expression **(Supplementary Table S5)**.

Nectin-4 expression is associated with reduced immune cell infiltration in PDAC.

Next, the correlation between ligand expression and intratumoral T cell infiltration and phenotypes was evaluated. CD155 expression was not associated with the distribution of T cell subsets in blood (**Fig. 3A**) and tumor (**Fig. 3B**). Further the expression of TIGIT, CD226, and CD96 in blood T cell subsets (**Fig. 3C**) was independent of CD155 tumor tissue expression, but PDAC-infiltrating Tconv and Treg showed decreased TIGIT expression in CD155-high PDAC (**Fig. 3D**). While the PDAC cohort with high CD155 expression was small, no significant difference in CD226 and CD96 expression was detected compared with CD155-low PDAC samples. All intratumoral T cell subsets in the CD155-high cohort showed a trend toward increased CD226 expression. Strikingly, Nectin-4-high tumors displayed no differences in the general T cell frequency and subset frequency in the blood (**Fig. 4A**), but a significantly reduced frequency of T cells among all immune cells in the tumor, but without alterations in T cell subset composition (**Fig. 4B**). Again, high Nectin-4 expression was not associated with changes of the ICR expression by blood T cell subsets (**Fig. 4C**), but PDAC-infiltrating Treg

showed increased TIGIT expression, with a similar trend for $CD8^+$ T cells and Tconv (**Fig. 4D**). Intratumoral T cells from Nectin-4-high PDAC had slightly reduced CD226 expression, but significantly reduced CD96 expression among all T cell subsets.

Nectin-4 is exclusively expressed by tumor cells in PDAC.

To further validate the relevance of Nectin-4 in PDAC, we analyzed 17 primary tumor and 9 liver metastasis samples using scRNA-Seq (**Fig. 5, Supplementary Fig. S3A-C**). *TIGIT*, *CD226,* and *CD96* were expressed by all T cell subsets and NK cells to varying degrees, with $CD8^+$ T cells exhibiting the highest expression of *CD96*, while Treg had high *TIGIT* expression in PDAC (**Fig. 5A**). Notably, *PVRL4* (Nectin-4) was expressed exclusively by tumor cells, while *PVRL2* (Nectin-2) was expressed by various cell types, including CAFs, myeloid, malignant epithelial, and endothelial cells. A low percentage of endothelial and tumor cells expressed *PVR* (CD155). Expression patterns were broadly similar between treatment-naive PDAC, PDAC treated with chemotherapy, and treatment-naive PDAC liver metastases (**Supplementary Fig. S3A**). Interestingly, while *PVR* and *PVRL4* were also expressed by tumor cells in PDAC liver metastases, the expression of *PVR* was significantly increased in the metastatic cells(**Supplementary Fig. S3B**), and *PVRL4* showed higher expression within the tumor cells from the primary tumor (**Fig. 5B**). *PVR* and *PVRL4* expression correlated negatively in PDAC (**Supplementary Fig. S3C**). Further, a trend for a negative correlation between *PVRL4,* but not *PVR,* and the proportion of cells per sample in the T cell compartment, a proxy for lymphocyte infiltration, was observed (**Fig. 5C, Supplementary Fig. S3C**).

Enfortumab vedotin has anti-tumor efficacy in PDAC PDOs.

Upon activation, T cells produce proinflammatory cytokines like IFN-γ and TNF-α, which are crucial for mediating antitumoral immune responses. To assess the effect of Nectin-4 on T cell function, we cultured activated T cells from PDAC patients in the presence of plate bound (pb) (n = 8) or solube Nectin-4 (sNectin-4, n = 4). After three days, T cells cultured with pbNectin-4 exhibited a markedly reduction of IFN-γ and TNF-α secretion, compared to the control without

Nectin-4 (**Fig. 6A**). In the presence of sNectin-4, cytokine expression was also significantly reduced, but to a lesser extent. Next, we tested several patient-derived PDAC organoids (PDO) for their Nectin-4 expression using RT-qPCR (**Fig. 6B**) and western blotting (**Fig. 6C**). PDAC PDOs showed varying *PVRL4* mRNA expression, which corresponded to Nectin-4 protein expression. Due to its tumor-specific and generally high expression in PDAC, Nectin-4 may be a potential therapeutic target. Therefore, we investigated the anti-tumor effiacacy of enfortumab vedotin (EV) in *in vitro* drug screens on PDAC PDOs. Therapeutic responses were compared to the effiacacy of the chemotherapy regimens FOLFIRINOX and gemcitabine plus paclitaxel (Gem/Pac). Here, a wide range of responses was observed for each treatment (**Fig. 6D**). Z scores of relative AUCs were calculated to detect different response patterns within the same line, demonstrating drug-sensitivity to EV in four (DD593, DD882, DD1391, and DD1404) PDAC PDOs (**Fig. 6E**). DD1391 and DD1404 showed sensitivity to all treatments, whereas DD728 was resistant. Interestingly, DD593 and DD882 exhibited resistance to either one or both chemotherapeutic regimens, while displaying sensitity to EV. To further explore the effect of EV on the chemotherapy-resistant PDOs DD593 and DD882, we evaluated apoptosis by caspase-3 staining. Strinkingly, after three days of incubation, DD593 and DD882 underwent early apoptosis upon treatment with EV, while treatment with FOLFIRINOX and Gem/Pac resulted in only a few apoptotic cells (**Fig. 6F**). Collectively, EV demonstrated antitumoral efficacy in approximately 50 % of PDAC PDOs.

DISCUSSION

TIGIT expression plays a central role in T cell exhaustion in human and murine PDAC (6, 9). Further, Treg have a higher abundance of TIGIT in the blood and within the tumor, which is consistent with an attenuated signal transduction response in Treg in comparison to effector T cell subsets (7). TIGIT acts as a counter-regulatory protein to CD226 by competing for binding to its primary ligand CD155 with higher affinity and by disrupting its homodimerization (5). Co-stimulation by CD226 is important for T cell anti-tumor function and is associated with a better response to immune checkpoint blockade in lung cancer and melanoma (14, 15), and it can even compensate for CD28 deficiency (16). Therefore, significantly reduced CD226 expression by intratumoral $CD8^+$ T cells observed in PDAC suggests an impaired ability for crucial co-stimulation. Interestingly, TIGIT and CD226 expression showed a negative correlation, further highlighting their functional interplay. Studies that originally suggested the involvement of the TIGIT axis in PDAC immune evasion highlighted CD155 by predicting its interaction with TIGIT within scRNA-seq data (6, 17). TIGIT/CD155 interaction promoted immune evasion in murine PDAC that was overcome by combinational immunotherapy, including TIGIT-blockade (9). Since murine TIGIT does not interact with murine Nectin-4 or other ligands, but only with murine CD155, classical mouse models are insufficient to study the TIGIT axis and conclusions that can be drawn are limited (18, 19). Therefore, we solely analyzed human samples and assessed ligands and ICR beyond TIGIT and CD155 to identify critical components within the network. High Nectin-4 expression has been detected in various solid tumors and was associated with unfavorable prognosis in esophageal and gastric cancer (20-22). Nectin-4 has been proposed as a diagnostic biomarker in lung and metastatic breast cancer (23, 24). Strikingly, Nectin-4 expression correlated negatively with T cell infiltration in the TCGA, scRNA-seq and IHC/flow cytometry data sets. Nectin-4 was associated with increased TIGIT expression by PDAC-infiltrating T cells, but not in blood T cells, indicating potential Nectin-4-derived immunosuppression via the TIGIT axis particularly in the PDAC tumor microenvironment. In contrast, tumor CD155 expression was associated with reduced TIGIT expression, suggesting an increased anti-tumor immunity in CD155 high tumors. CD155

may provide co-stimulation via interaction with CD226, whereas Nectin-4 appears to solely interact with TIGIT (5, 18). Our study provides important new human data to expand our knowledge of the TIGIT axis in PDAC by suggesting that Nectin-4, rather than CD155, is the central ligand for TIGIT axis-mediated PDAC immune evasion by elucidating its potential as therapeutic target. Despite both serving as TIGIT ligands, their opposing prognostic effects suggest distinct immunomodulatory functions that warrant ligand-specific therapeutic targeting. When cultivated with Nectin-4, T cells produced significantly fewer effector cytokines. Interestingly, this effect was more pronounced with plate bound, than soluble Nectin-4. TIGIT expression by T cells was similar across all patients, indicating that observed immunosuppressive effects were not caused by differential TIGIT expression, but may rather be dependent on the mode of Nectin-4 engagement with T cells. Targeting Nectin-4 may offer an additional treatment approach for PDAC that merits clinical assessment. Expression of Nectin-4 is found in the embryo and placenta during fetal development and is rare in healthy adult tissues, but often overexpressed in tumor tissues (25). It is an attractive therapeutic target in PDAC due to its highly tumor cell-specific expression. In a multi-cancer study, PDAC had the third highest Nectin-4 expression by immunohistochemistry, after urothelial and breast cancer (20). In addition, Nectin-4 overexpression has frequently been linked to reduced survival in several other cancers (26). The antibody-drug conjugate enfortumab vedotin (EV), which binds Nectin-4 and delivers a microtubule disrupting agent, proved beneficial as a second-line treatment after platinum-based chemotherapy and PD-1- or PD-L1-blockade in locally advanced or metastatic urothelial carcinoma (27). The EPIC trial (NCT05915351) is currently investigating the efficacy of EV in metastatic PDAC (28). Patient-derived organoids (PDO) recapitulate the genetic landscape of their parental tumors and have high predictive accuracy when studying patient-specific responses (29-32). Using several PDOs derived from PDAC patients, we showed anti-tumor efficacy of EV, particularly in several chemoresistant PDOs, indicating the potential of EV as a therapeutic alternative for PDAC patients. In conclusion, our study provides further evidence for the involvement of the TIGIT axis in PDAC immune evasion and uncovers Nectin-4 instead of CD155 as the most clinically relevant ligand,

which also presented as a strong risk factor for reduced overall survival. While supporting TIGIT blockade as an immunotherapeutic strategy, this study provides the rationale to target Nectin-4 in PDAC, which merits clinical evaluation.

METHODS

Sex as a biological variable. Our study examined samples from male and female PDAC patients and our findings are expected to be relevant for more than one sex.

Patient Samples. All human samples were obtained from patients of the University Hospital Carl Gustav Carus. For flow cytometry and *in vitro* studies, fresh tumor specimens and matched blood samples were collected from PDAC patients, who underwent surgery between 2018 and 2024. Blood was drawn before surgical incision and fresh tumor specimens were collected immediately after resection and evaluated by a trained pathologist. For IHC staining, formalin-fixed and paraffin-embedded PDAC tissue sections were obtained from the Institute of Pathology of the University Hospital Dresden. These samples matched fresh tumors, which had been processed for flow cytometry. The clinical stage of the tumors were classified according to the TNM system (UICC; Edition 8).

Multicolor Flow Cytometry. Single-cell suspensions of blood and PDAC samples for flow cytometry were prepared as described previously (7). Cells were stained both extra- and intracellularly with monoclonal antibodies listed in **Supplementary Table S6**. Cells were fixed and permeabilized for intracellular staining with eBioscience™ FOXP3/Transcription Factor Staining Buffer Set (Thermo Fisher) according to the manufacturer's protocol. Flow cytometry was performed using a LSR Fortessa flow cytometer (BD Biosciences, RRID:SCR_018655). Data was analyzed using FlowJo v10.7.1 (Treestar, Ashland, OR, RRID:SCR_008520). A minimum number of 200 cells was set as a prerequisite for the subset analysis. Each patient was analyzed individually according to a previously shown gating hierarchy (7).

Immunohistochemistry. Sections of formalin-fixed, paraffin-embedded PDAC tissues were deparaffinized and rehydrated. Antigen retrieval was performed by boiling the slides in sodium citrate buffer (pH 6.0) and DAKO Protein Block (Agilent) was used to block nonspecific binding. Anti-CD155 (ab123252, Abcam, RRID:AB_10975440) or anti-Nectin-4 (PA5-30837,

Invitrogen, RRID:AB_2548311), both 1:200 in Dako Antibody Diluent (Agilent), were applied at 4°C overnight. Anti-rabbit SignalStain boost IHC Detection Reagent (Cell Signaling Technology) was used as a secondary detection antibody for 30min at room temperature. The ImmPACT™ DAB Peroxidase Substrate Kit (Vector Labs) was used according to the manufacturer's instructions for a chromogenic reaction. Counterstaining was performed with Mayer's hematoxylin (Clin-Tech). A trained pathologist calculated the immunoreactive score (IRS) by multiplying the staining intensity (0-3) with the proportion of positive tumor cells (0-4) (33). An IRS of 0-4 was considered as low expression, and an IRS of 6-12 as high. Representative images were taken with the ECHO Revolve microscope (RRID:SCR_026523) at 10x magnification.

Single-cell RNA Sequencing. The scRNA-seq data has previously been published (17). Samples were collected from 26 PDAC patients, including 17 primary tumors and 9 liver metastases at the Perlmutter Cancer Center at NYU Langone Health after obtaining informed written consent. Single-cell suspensions were processed for 10x Genomics by the Genome Technology Center at the NYU School of Medicine per the manufacturer's guidelines. Sequencing results were de-multiplexed and converted to FASTQ format using Illumina bcl2fastq software. The 10x Genomics Cell Ranger 5.0.1 software suite (34) was used to perform sample de-multiplexing, barcode processing, and single-cell 3' gene counting aligned to the hg38/GRCh38 reference genome. Only confidently mapped, non-PCR duplicates with valid barcodes and unique molecular identifiers were used to generate the gene-barcode matrix. Clusters were identified based on common marker genes, for various cell types, the most prominent of which are listed here: $CD8^+$ T cells (*CD3E*, *CD8*), Tconvs (*CD3E*, *CD4*, *FOXP3*-), Tregs (*CD3E*, *CD4*, *FOXP3*), NK (*NCAM1*), B/Plasma (*CD79A*), Mast (*KIT*), MDSC (*S100A8*, *S100A9*, *S100A12*), monocytes (*FGCR3A*, *CDKN1C*), macrophages (*CD68*), pDC (*LILRA4*, *PLD4*), cDC (*CD1C*), iCAFs (*C3*, *C7*, *CFD*, *PTGDS*), myCAFs (*ACTA2*, *MMP11*, *COL10A1*-), endothelial (*PECAM1*, *VWF*), and epithelial (*KRT19*). InferCNV version 1.8.1 was run at a sample level to differentiate between malignant and nonmalignant pancreatic epithelial

cells. Further analyses, including the generation of the dot plots and violin plots, were performed using Seurat (35) and scooter (36). For more detailed information on the sample set, sample preparation, and initial data processing, see reference (17).

TCGA Data Analysis. The PAAD dataset (https://portal.gdc.cancer.gov/) was analyzed for the correlation between different genes of interest, assessing the Spearman's rank correlation coefficients. Standardized expression levels from 146 PDAC patients were depicted in a heatmap, ranked by *PVRL4* expression, using GraphPad Prism 9.3.1 (San Diego, California USA, www.graphpad.com, RRID:SCR_002798).

***In vitro* T cell Assay.** Cryopreserved PBMC samples from PDAC patients who underwent neoadjuvant chemotherapy (FOLFIRINOX or Gemcitabine plus Paclitaxel) were thawed in prewarmed DPBS (Sigma Aldrich) supplemented with fetal calf serum (Gibco). Pan T cells were isolated trough negative selection using the Pan T cell Isolation Kit (Miltenyi). One day prior seeding, 96-well plates (U-bottom, Greiner Bio-One) were coated overnight with 10 µg/ml anti-CD3 (BioLegend, RRID:AB_11146991), 10 µg/ml anti-CD28 (BioLegend, RRID:AB_11148949) together with 20 µg/ml recombinant Nectin-4 protein (R&D Systems). Pan T cells were plated at $1x10^5$ cells per well in T cell medium (RPMI-1640 (Gibco) supplemented with 10 % human AB serum (Sigma Aldrich), 2.5 % HEPES (Gibco) and 1 % Pen/Strep (Gibco)) and incubated for 72 h. In addition, soluble recombinant Nectin-4 protein was added to the culture medium at a final concentration of 20 µg/ml at the time of plating. No medium change was performed during the incubation period. The supernatants were collected and cytokines IFN-γ and TNF-α were measured using the Th1, Th2, Th17 CBA kit (BD) on a LSR Fortessa (BD Biosciences, RRID:SCR_018655).

Gene Expression Analysis. Total mRNA was obtained from each PDO line using RNeasy Kit (QUIAGEN) and genomic DNA was digested using RNase-free DNase Kit (QUIAGEN). qRT-PCR was performed with GoTaq® qPCR Kit (Promega) on a StepOnePlus RT PCR System

(Applied Biosystems). *PVRL4* expression was analyzed using cDNA synthesized from each PDO line with the MultiScribeTM Reverse Transcriptase Kit (Applied Biosystems). The genes *GAPDH* and *RPL13* were chosen as internal controls. For both control genes and the target gene *PVRL4*, QuantiNova LNA PCR Assays (QUIAGEN) were used (HS_GAPDH_1799381, HS_RPL13_1769191, HS_NECTIN4_1411019). Amplification reactions were performed in duplicates and relative gene expression was evaluated using comparative ΔCT method.

Western Blot. Proteins were obtained from each PDO line by resuspending cell pellets in lysis buffer (50 mM Tris-HCl with pH 8, 150 mM NaCl, 1 % NP-40, 0.5 % sodium deoxycholate, 0.1 % SDS) with protease and phosphatase inhibitors (Thermo Fisher Scientific). Lysates were loaded in 20 µg protein per well and separated by electrophoresis on a SDS-PAGE gel (Invitrogen) and then transferred onto a PVDF membrane. The membrane was incubated overnight at 4°C with Nectin-4 antibody (#17402, Cell Signaling Technology, RRID:AB_2798785). GAPDH antibody (#2118S, Cell Signaling Technology, RRID:AB_561053) and horseradish peroxidase-conjugated secondary antibody (#7074S, Cell Signaling Technology, RRID:AB_2099233) were incubated for 1 h at room temperature.

Human PDAC Organoids. PDOs were generated from surgical resection specimens as described previously (29). Briefly, tumor samples were cut into small pieces and digested using dispase II (2.5 mg/ml, Roche) and collagenase II (0.625 mg/ml, Sigma-Aldrich) in DMEM/F12+++ medium (DMEM/F12 (Invitrogen) supplemented with 1x HEPES (Invitrogen), 1x Pen/Strep (Invitrogen) and 1x GlutaMAX (Invitrogen)) at 37°C. The cell pellet was resuspended in GFR Matrigel (Corning). PDAC PDOs were cultivated in PDAC organoid medium DMEM/F12+++ supplemented with Wnt3a-conditioned medium (50 % v/v), Noggin-conditioned medium (10 % v/v), R-spondin-conditioned medium (10 % v/v), B27 (1x, Invitrogen), nicotinamide (10 mM, Sigma-Aldrich), gastrin (1 nM, Sigma-Aldrich), N-acetyl-L-cysteine (1 mM, Sigma-Aldrich), Primocin (1 mg/ml, InvivoGen), recombinant murine epidermal growth factor (mEGF, 50 ng/ml, Invitrogen), recombinant human fibroblast growth

factor 10 (hFGF-10, 100 ng/ml, PeproTech), A-83-01 (0.5 µM, Tocris Bioscience), and N2 (1x, Invitrogen). For the first 2-6 passages, PDAC PDOs were supplemented with Y-27632 (10 µM, Sigma-Aldrich). Depending on the growth rate, PDAC PDOs were passaged one to two times a week with a ratio of 1:2 to 1:4.

***In vitro* Drug Assays.** PDAC PDOs were passaged on day 0 and supplemented with dispase II (1 mg/ml, Roche) on day 1, following a 2 h incubation to enzymatically digest the matrigel. PDAC PDOs in suspension were then filtered by size (pluriStrainer, pluriSelect). Organoids between 20 µm - 50 µm in size were plated as triplicates in 384 well plates (µClear white, Greiner Bio-One) in 15 µl 75 % Matrigel. Chemotherapeutics were provided by the local pharmacy department at the University Hospital Dresden and used as described earlier (29). Briefly, the dilution step *n* for FOLFIRINOX contained 10 µM irinotecan plus 35 µM oxaliplatin plus 35 µM 5-FU. The dilution step *n* for Gem/Pac contained 11.2 µM gemcitabine plus 7.2 µM paclitaxel. The antibody-drug conjugate enfortumab vedotin was used in serial dilution from 0.1 mM to 600 mM. To evaluate the effect of single and combination drugs, cell viability was measured using CellTiter Glo 3D (Promega) after a total treatment of 6 days. Luminescence was measured using a Varioskan LUX (Thermo Fisher Scientific). Every single and combination drug treatment was performed two times in independent experiments and averaged for dose response curves and following analyses.

Live Cell Imaging. PDAC PDOs in suspension were obtained as described above. PDAC PDOs were filtered by size and organoids between 50 - 100 µm im size were plated as duplicates in 384 well plates (Corning) in 15 µl 15 % Matrigel. Based on the dose response curves for each single and combination drug, mean IC50 values were calculated and the next lower previously applied concentration was used for treatment (FOLFIRINOX n/9, Gem/Pac n/4, enfortumab vedotin 10 µg/ml). After two days of incubation, Caspase-3 dye BioTracker™ NucView® 488 Green (Thermo Fisher Scientific) was added to each well with a final

concentration of 5 µM. PDOs were imaged on day 3 with Operetta CLS (Perkin Elmer, RRID:SCR_018810).

Statistical Analysis. Data is shown as the median in scatterplots or mean in bar graphs. Unpaired or paired two-sided t-tests with Holm-Šídák correction were used as applicable. Wilcoxon signed-rank test was used for comparison of expression level within scRNA-seq data. Kaplan-Meier plots for survival analysis of R0-resected patients were generated with GraphPad Prism 9.3.1 and evaluated by the log-rank test. A multivariate Cox proportional-hazards regression considering T, N, and M stage, resection margin (R), neoadjuvant chemotherapy, age, and sex was used to define HRs for intratumoral CD155 or Nectin-4 expression by using R Environment for Statistical Computing. Patients who died within 30 days after surgery were excluded from survival analysis. Fisher's exact test was used to compare characteristics of the control and PDAC cohort and CD155 or Nectin-4 IRS distributions as a function of clinical characteristics. Pearson correlation coefficient was used to analyze the correlation between the expression of TIGIT, CD226, and CD96 within the different T cell subsets or within the scRNA-seq expression data. $P \leq 0.05$ was considered statistically significant, except for the correlation matrices, where $P \leq 0.01$ was considered significant to account for multiple comparisons. All PDO lines were analyzed in two independent experiments for each single and combination drug. Values were averaged and standard deviation (SD) was calculated. Using GraphPad Prism, dose response curves were generated and IC50 values and area under the curve (AUC) were determined. For AUC z-score normalization, relative AUC (AUCrel) was calculated from the quotient of AUC of dose response curve normalized to AUC 100 % which represents the relative viability as 100 %. The formula $z = (x - \mu)/\sigma$ was used, where x is the mean AUCrel from the PDO line tested in two individual experiments, µ is the mean AUCrel from all PDO lines analyzed, and σ is the standard deviation from all PDO lines analyzed. For comparison of cytokine expression of T cells, unpaired two-sided t-test with Welch's correction were applied. GraphPad Prism

(GraphPad Software, RRID:SCR_002798) was used and $P \leq 0.05$ was considered statistically significant.

Study Approval. All human samples were obtained from patients of the University Hospital Carl Gustav Carus, who gave written consent to a protocol approved by the Ethics Committee of the Technische Universität Dresden (No. EK446112017).

Data Availability. All supporting data values associated with the main manuscript and supplement material, including values for all data points shown in graphs and values behind any reported means, are provided in the supporting data values file. The raw scRNA-seq data used for this project is available under GEO accession number GSE205013 (17). The raw flow cytometry data of this study is available from the corresponding author upon reasonable request.

AUTHOR CONTRIBUTIONS

MH, LS and AMS conceived this study. MH, CB, EAK, and JG developed the methodology. MH and CB performed the experiments and analyzed the data. EAK and SK analyzed the scRNA-seq data. US evaluated and scored the IHC staining. MH, CB, SC, LS and AMS curated the data. LS and AMS acquired funding. JW provided the research facilities. MH and CB wrote the manuscript. All authors reviewed the manuscript. Among both co-first authors, authorship order was determined according to contribution to study conception by MH.

ACKNOWLEDGMENTS

We thank Heike Polster for her assistance in acquiring human blood, the Institute of Pathology in Dresden members for their help in obtaining tumor specimens, and Beatrix Jahnke, Valeria Lozovanu, and Alexander Hennig for excellent technical assistance. This work was supported by the Ernst-Jung Stiftung (LS), Monika Kutzner Stiftung (AMS), German Research Foundation (DFG; SE2980/5-1; LS), the German Cancer Consortium (DKTK; AMS), Medical Faculty Carl Gustav Carus Technische Universität Dresden (MH, AMS), the Else Kröner-Fresenius-Stiftung (Else Kröner Clinician Scientist Professorship; LS), and the Federal Ministry of Education and Research (Advanced Clinician Scientist Program CAMINO Dresden; AMS).

REFERENCES

1. Siegel RL, et al. Cancer statistics, 2023. *CA Cancer J Clin.* 2023;73(1):17–48.
2. Ho WJ, et al. The tumour microenvironment in pancreatic cancer - clinical challenges and opportunities. *Nat Rev Clin Oncol.* 2020;17(9):527–40.
3. Yousuf S, et al. Spatially Resolved Multi-Omics Single-Cell Analyses Inform Mechanisms of Immune Dysfunction in Pancreatic Cancer. *Gastroenterology.* 2023.
4. Muller M, et al. The Immune Landscape of Human Pancreatic Ductal Carcinoma: Key Players, Clinical Implications, and Challenges. *Cancers (Basel).* 2022;14(4).
5. Chiang EY, and Mellman I. TIGIT-CD226-PVR axis: advancing immune checkpoint blockade for cancer immunotherapy. *J Immunother Cancer.* 2022;10(4).
6. Steele NG, et al. Multimodal Mapping of the Tumor and Peripheral Blood Immune Landscape in Human Pancreatic Cancer. *Nat Cancer.* 2020;1(11):1097–112.
7. Heiduk M, et al. TIGIT Expression Delineates T-cell Populations with Distinct Functional and Prognostic Impact in Pancreatic Cancer. *Clin Cancer Res.* 2023;29(14):2638–50.
8. Cui Zhou D, et al. Spatially restricted drivers and transitional cell populations cooperate with the microenvironment in untreated and chemo-resistant pancreatic cancer. *Nat Genet.* 2022;54(9):1390–405.
9. Freed-Pastor WA, et al. The CD155/TIGIT axis promotes and maintains immune evasion in neoantigen-expressing pancreatic cancer. *Cancer Cell.* 2021;39(10):1342–60.e14.
10. Blake SJ, et al. Molecular Pathways: Targeting CD96 and TIGIT for Cancer Immunotherapy. *Clin Cancer Res.* 2016;22(21):5183–8.
11. Li J, et al. High Levels of Eomes Promote Exhaustion of Anti-tumor CD8(+) T Cells. *Front Immunol.* 2018;9:2981.
12. De Monte L, et al. Intratumor T helper type 2 cell infiltrate correlates with cancer-associated fibroblast thymic stromal lymphopoietin production and reduced survival in pancreatic cancer. *J Exp Med.* 2011;208(3):469–78.
13. Manero-Rupérez N, et al. The Galectin Family as Molecular Targets: Hopes for Defeating Pancreatic Cancer. *Cells.* 2020;9(3).
14. Banta KL, et al. Mechanistic convergence of the TIGIT and PD-1 inhibitory pathways necessitates co-blockade to optimize anti-tumor CD8(+) T cell responses. *Immunity.* 2022;55(3):512–26.e9.
15. Braun M, et al. CD155 on Tumor Cells Drives Resistance to Immunotherapy by Inducing the Degradation of the Activating Receptor CD226 in CD8(+) T Cells. *Immunity.* 2020;53(4):805–23.e15.
16. Béziat V, et al. Humans with inherited T cell CD28 deficiency are susceptible to skin papillomaviruses but are otherwise healthy. *Cell.* 2021;184(14):3812–28.e30.
17. Werba G, et al. Single-cell RNA sequencing reveals the effects of chemotherapy on human pancreatic adenocarcinoma and its tumor microenvironment. *Nat Commun.* 2023;14(1):797.
18. Reches A, et al. Nectin4 is a novel TIGIT ligand which combines checkpoint inhibition and tumor specificity. *J Immunother Cancer.* 2020;8(1).
19. Rishiq A, et al. Studying TIGIT activity against tumors through the generation of knockout mice. *Oncoimmunology.* 2023;12(1):2217735.
20. Challita-Eid PM, et al. Enfortumab Vedotin Antibody-Drug Conjugate Targeting Nectin-4 Is a Highly Potent Therapeutic Agent in Multiple Preclinical Cancer Models. *Cancer Res.* 2016;76(10):3003–13.
21. Deng H, et al. Over-expression of Nectin-4 promotes progression of esophageal cancer and correlates with poor prognosis of the patients. *Cancer Cell Int.* 2019;19:106.
22. Zhang Y, et al. High expression of Nectin-4 is associated with unfavorable prognosis in gastric cancer. *Oncol Lett.* 2018;15(6):8789–95.
23. Takano A, et al. Identification of nectin-4 oncoprotein as a diagnostic and therapeutic target for lung cancer. *Cancer Res.* 2009;69(16):6694–703.
24. M MR, et al. Nectin-4: a new prognostic biomarker for efficient therapeutic targeting of primary and metastatic triple-negative breast cancer. *Ann Oncol.* 2017;28(4):769–76.

25. Bouleftour W, et al. Nectin-4: a Tumor Cell Target and Status of Inhibitor Development. *Curr Oncol Rep.* 2023;25(3):181–8.
26. Liu R, et al. Prognostic value of nectin-4 in human cancers: A meta-analysis. *Front Oncol.* 2023;13:1081655.
27. Powles T, et al. Enfortumab Vedotin in Previously Treated Advanced Urothelial Carcinoma. *N Engl J Med.* 2021;384(12):1125–35.
28. Kasi A, et al. A phase II open-label study of enfortumab vedotin in patients with previously treated locally advanced, recurrent, or metastatic pancreatic adenocarcinoma (EPIC). *Journal of Clinical Oncology.* 2024;42(3_suppl):TPS719–TPS.
29. Hennig A, et al. Detecting drug resistance in pancreatic cancer organoids guides optimized chemotherapy treatment. *The Journal of Pathology.* 2022;257(5):607–19.
30. Schmäche T, et al. Stratifying esophago-gastric cancer treatment using a patient-derived organoid-based threshold. *Mol Cancer.* 2024;23(1):10.
31. Farshadi EA, et al. Tumor organoids improve mutation detection of pancreatic ductal adenocarcinoma. *Scientific Reports.* 2024;14(1):25468.
32. Wang E, et al. Patient-derived organoids (PDOs) and PDO-derived xenografts (PDOXs): New opportunities in establishing faithful pre-clinical cancer models. *J Natl Cancer Cent.* 2022;2(4):263–76.
33. Remmele W, and Stegner HE. [Recommendation for uniform definition of an immunoreactive score (IRS) for immunohistochemical estrogen receptor detection (ER-ICA) in breast cancer tissue]. *Pathologe.* 1987;8(3):138–40.
34. Zheng GX, et al. Massively parallel digital transcriptional profiling of single cells. *Nat Commun.* 2017;8:14049.
35. Butler A, et al. Integrating single-cell transcriptomic data across different conditions, technologies, and species. *Nat Biotechnol.* 2018;36(5):411–20.
36. Dolgalev I, and Yeaton A. Scooter: streamlined scRNA-seq analysis pipeline. 2021.

FIGURE LEGENDS

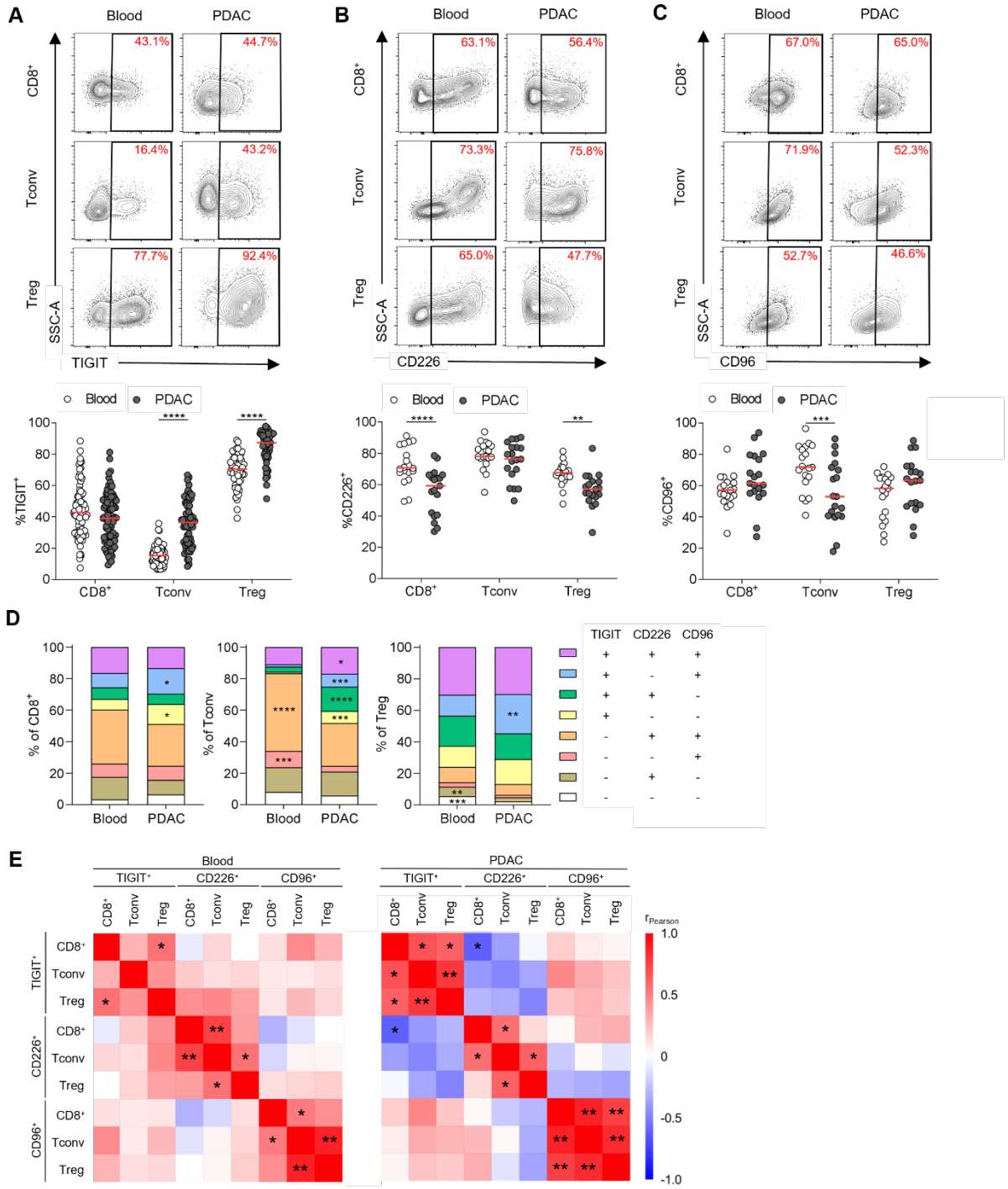

Figure 1. TIGIT, CD226, and CD96 are expressed by tumor-infiltrating T cells. (**A**) Representative contour flow plots for expression of TIGIT and percentage of TIGIT by $CD8^+$ T cells, Tconv and Treg in matched blood and PDAC (n = 84). (**B**) Representative contour flow plots for expression of CD226 and percentage of CD226 by $CD8^+$ T cells, Tconv and Treg in matched blood and PDAC (n = 19). (**C**) Representative contour flow plots for expression of CD96 and percentage of CD96 by $CD8^+$ T cells, Tconv and Treg in matched blood and PDAC (n = 19). Each point represents data from one patient. Medians are shown as horizontal red lines. Unpaired and paired two-sided t tests with Holm-Šídák correction respectively (**D**) Stacked columns showing the mean co-expression of TIGIT, CD226 and CD96 among $CD8^+$ T cells, Tconv and Treg (from left to right) in blood versus PDAC. Significantly increased subsets are indicated by the respective asterisk. *, $P < 0.05$; **, $P < 0.01$; ***, $P < 0.001$;

****, $P < 0.0001$. (**E**) Heatmap showing Pearson correlation coefficient ($r_{Pearson}$) for correlation between ICR expressions by indicated T cell subsets in blood (left) and PDAC (right). To correct for multiple comparison in correlation analysis, significance levels were set at *, $P < 0.01$; **, $P < 0.001$.

Figure 2

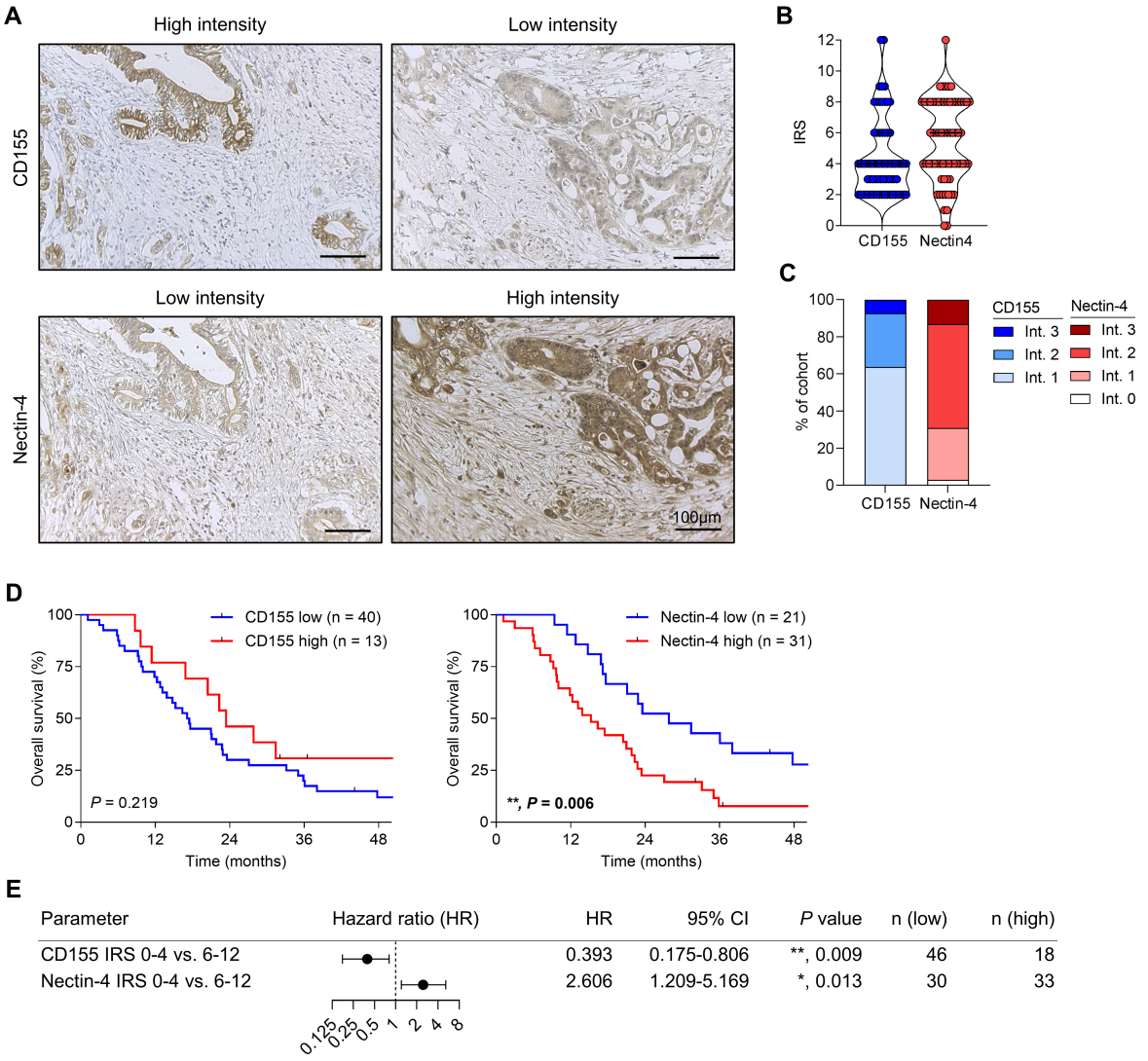

Figure 2. Nectin-4 expression is associated with poor outcome in PDAC. (**A**) Representative images of CD155 (top) and Nectin-4 (bottom) immunohistochemistry staining with low and high intensity. Scale bar is depicted. (**B**) Dot plot showing the distribution of immune reactive scores (IRS; CD155, n = 69; Nectin-4, n = 68). (**C**) Stacked columns depicting the proportion of patients with CD155 and Nectin-4 expression according to intensity. (**D**) Kaplan-Meier analysis of overall survival of R0-resected PDAC patients according to low or high CD155 (left) or Nectin-4 (right) expression. *P*-values of log rank test are indicated. (**E**) Table and forest plot depicting survival hazard ratios (HR) with 95 % confidence interval (CI) of CD155 and Nectin-4 IRS in multivariate Cox proportional hazards regression analysis including both R0- and R1-resected patients, shown as a function of clinicopathological parameters. *P*-values are depicted. *, $P < 0.05$; **, $P < 0.01$.

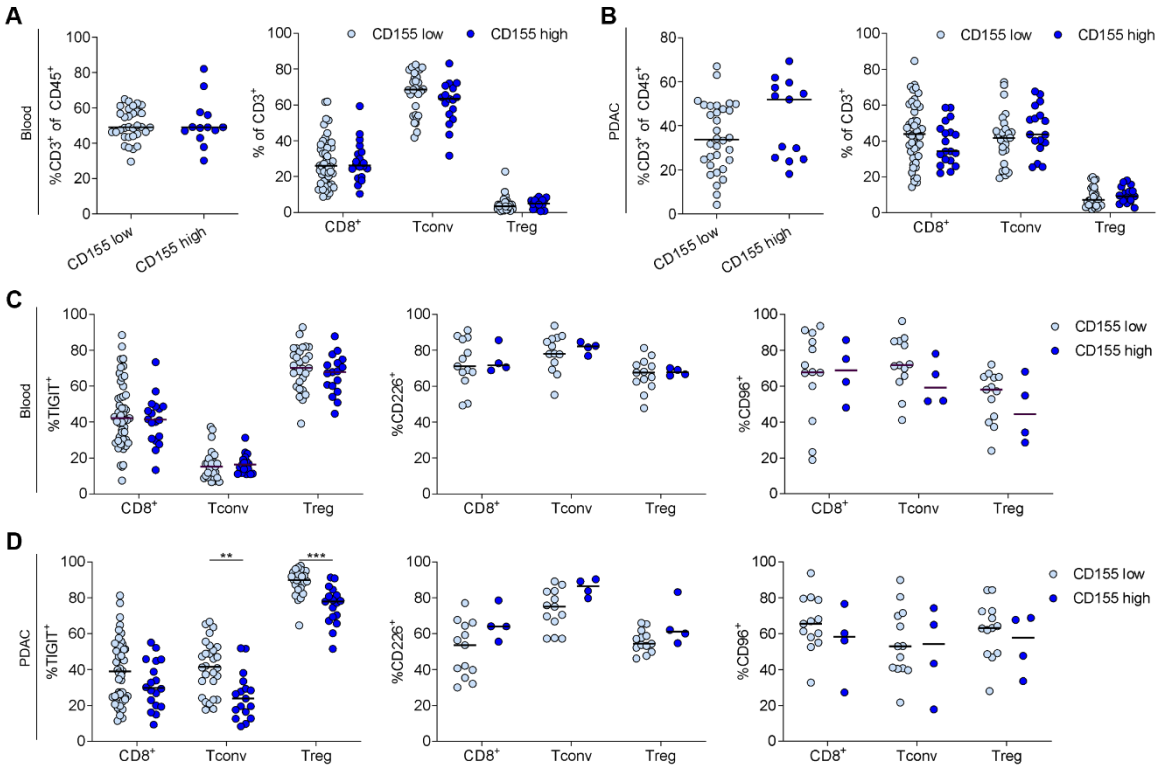

Figure 3. CD155 expression is associated with reduced TIGIT expression by PDAC-infiltrating Tconv and Treg cells. (**A**) Percentage of T cells among all immune cells (left) and percentage of indicated T cell subsets among all T cells (right) in blood and (**B**) PDAC for low and high CD155 expression (n = 69). (**C**) Percentage of TIGIT, CD226 and CD96 expression (from left to right) for indicated T cell subsets in blood and (**D**) PDAC for low and high CD155 expression. Each point represents data from one patient. Medians are shown as horizontal lines. Unpaired two-sided t tests with Holm-Šídák correction respectively. **, $P < 0.01$; ***, $P < 0.001$.

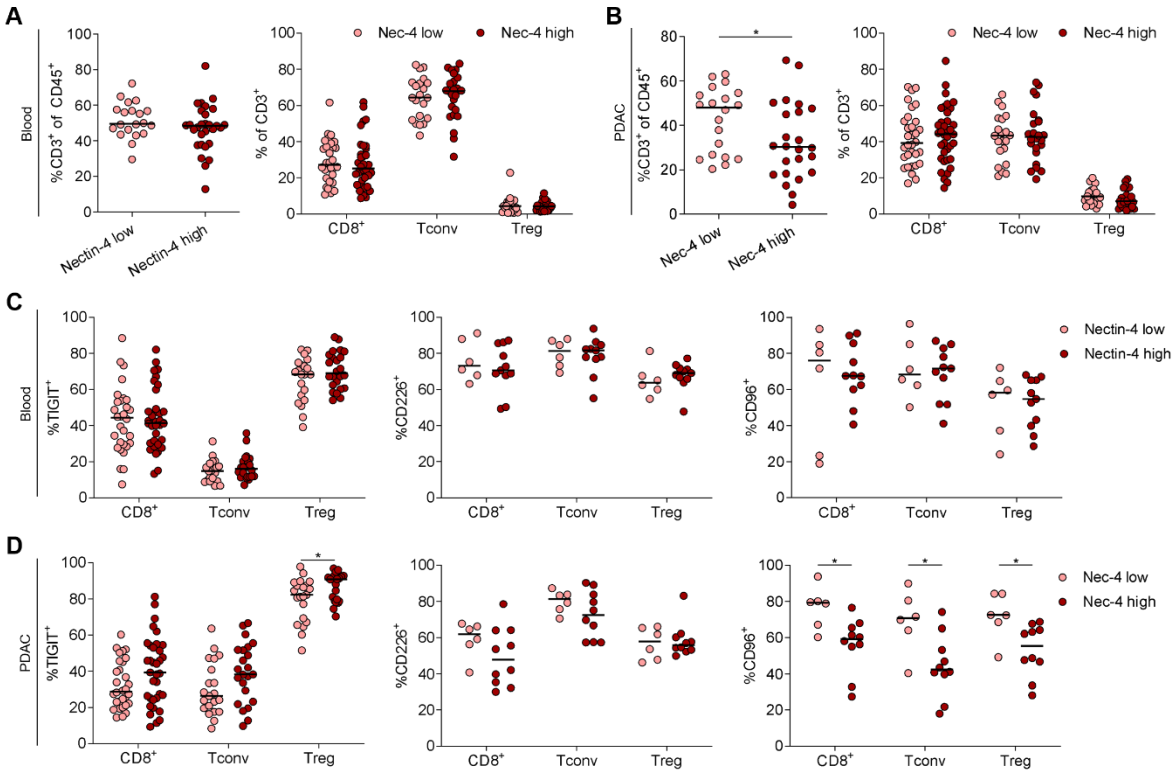

Figure 4. Nectin-4 expression is associated with reduced immune cell infiltration in PDAC. (**A**) Percentage of T cells among all immune cells (left) and percentage of indicated T cell subsets among all T cells (right) in blood and (**B**) PDAC for low and high Nectin-4 expression (n = 68). (**C**) Percentage of TIGIT, CD226 and CD96 expression (from left to right) for indicated T cell subsets in blood and (**D**) PDAC for low and high Nectin-4 expression. Each point represents data from one patient. Medians are shown as horizontal lines. Unpaired two-sided t tests with Holm-Šídák correction respectively. *, $P < 0.05$.

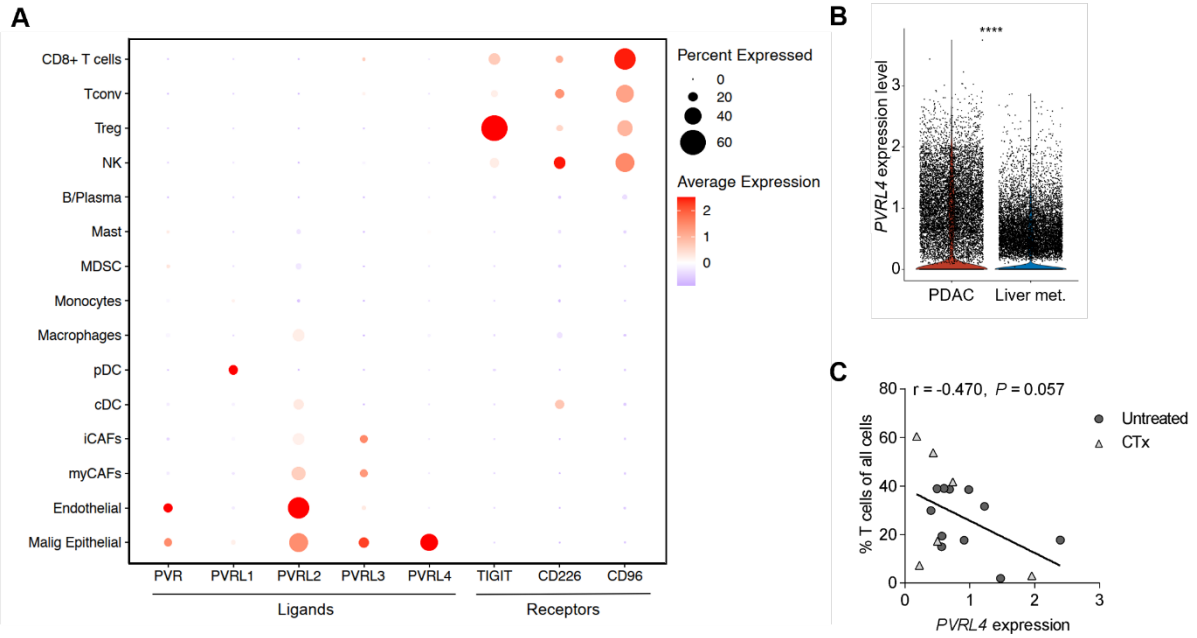

Figure 5. Nectin-4 is exclusively expressed by tumor cells in PDAC. (**A**) Dot plot depicting gene expression of TIGIT family receptors and ligands in several compartments within human primary PDAC (n = 17). The dot size represents the percentage of cells expressing the gene and the color represents the average expression within those cells. (**B**) Violin plot of *PVRL4* expression in all malignant epithelial cells in primary PDAC (n = 11) compared to PDAC liver metastases (n = 9) from treatment-naive patients. (**C**) Scatterplot showing the correlation between *PVRL4* expression in malignant epithelial cells and percentage of T cells among all analyzed cells per sample in treatment-naive (n = 11) and chemotherapeutically treated (n = 6) primary PDAC. Pearson correlation coefficients and *P*-values are depicted. Each dot represents one sample. Wilcoxon signed-rank test for comparison of expression levels. ****, $P < 0.0001$.

Figure 6

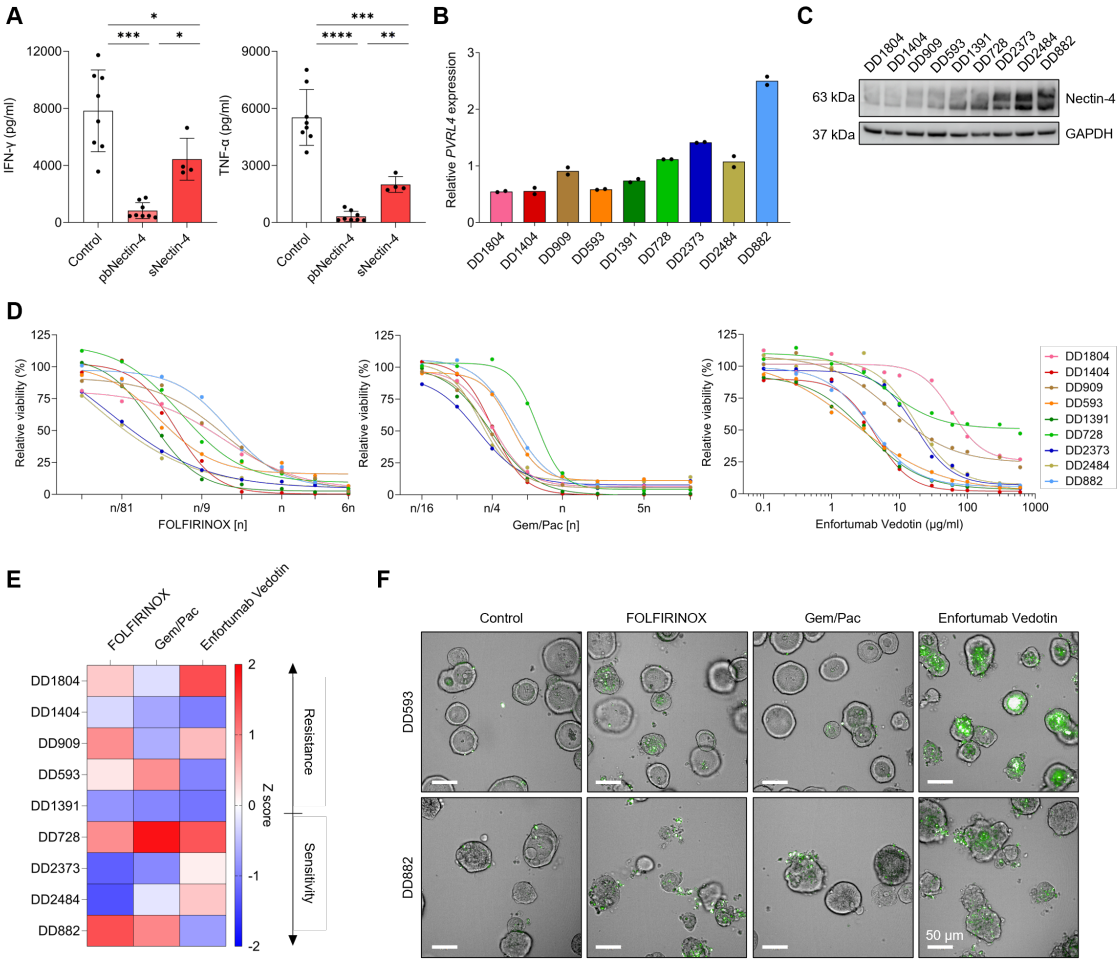

Figure 6. Enfortumab vedotin has anti-tumor efficacy in PDAC PDOs. (**A**) IFN-γ and TNF-α production by peripheral T cells from PDAC patients after *in vitro* stimulation with anti-CD3 and anti-CD28 in the presence of plate-bound (pb, n = 8) or soluble (s, n = 4) Nectin-4. Each point represents data from one patient. Bars indicate mean ± standard deviation (SD). Unpaired two-sided t tests with Welch's correction respectively. *P*-values are depicted. *, $P < 0.05$; **, $P < 0.001$; ***, $P < 0.001$; ****, $P < 0.0001$. (**B**) Representative expression level of *PVRL4* by RT-qPCR (bars indicate mean of technical duplicates) and (**C**) Nectin-4 expression in PDAC PDOs by western blot. **(D)** Dose response curves from PDAC PDOs treated with FOLFIRINOX, gemcitabine plus paclitaxel (Gem/Pac), or enfortumab vedotin. The relative viability in % at a given drug concentration of two independent biological replicates is shown. **(E)** Z scores generated from relative AUC from dose response curves from PDAC PDOs either treated with FOLFIRINOX, Gem/Pac, or enfortumab vedotin. **(F)** Representative images of two PDAC PDOs either treated with the standard regimen FOLFIRINOX, Gem/Pac, or enfortumab vedotin. PDOs were stained with caspase-3 dye profiling apoptosis (green) and imaged after three days. Scale bar is depicted.